

Kinetic Trans-assembly of DNA Nanostructures

Jihoon Shin¹, Junghoon Kim², Sung Ha Park^{2,3}, and Tai Hwan Ha^{1,4,*}

¹Hazards Monitoring Bionano Research Center, Korea Research Institute of Bioscience and Biotechnology (KRIBB), Daejeon 34141, Korea

²Department of Physics, Sungkyunkwan University, Suwon 16419, Korea

³Sungkyunkwan Advanced Institute of Nanotechnology (SAINT), Sungkyunkwan University, Suwon 16419, Korea

⁴Department of Nanobiotechnology, KRIBB School of Biotechnology, Korea University of Science and Technology (UST), Daejeon 34113, Korea

*email: taihwan@kribb.re.kr

Abstract

The central dogma of molecular biology is the principal framework for understanding how nucleic acid information is propagated and used by living systems to create complex biomolecules. Here, by integrating the structural and dynamic paradigms of DNA nanotechnology, we present a rationally designed synthetic platform which functions in an analogous manner to create complex DNA nanostructures. Starting from one type of DNA nanostructure, DNA strand displacement circuits were designed to interact and pass along the information encoded in the initial structure to mediate the self-assembly of a different type of structure, the final output structure depending on the type of circuit triggered. Using this concept of a DNA structure ‘trans-assembling’ a different DNA structure through non-local strand displacement circuitry, four different schemes were implemented. Specifically, 1D ladder and 2D double-crossover (DX) lattices were designed to kinetically trigger DNA circuits to activate polymerization of either ring structures or another type of DX lattice under enzyme-free, isothermal conditions. In each scheme, the desired multilayer reaction pathway was activated, among multiple possible pathways, ultimately leading to the downstream self-assembly of the correct output structure.

1 Introduction

The spatiotemporal control of information in any living system is central to its sustenance. At the cellular level, extra and intracellular information is carefully processed by a network of biochemical circuitry to orchestrate a variety of required functions.¹ One such process is the regulation of proteins such as actin and tubulin which themselves polymerize into higher-order microfilaments and microtubules.²⁻⁴ These structures have been studied extensively due to the multiple key roles they play during the life cycle of the cell, *e.g.* cytokinesis,² cell motility,⁵ mechanical and structural stability,⁶ intracellular transport,^{7,8} and DNA segregation.⁹ Given the importance of these and other structures in the cell, it naturally follows that being able to not only synthesize them but also regulate their synthesis would be critical developments in synthetic biology and molecular engineering.

To tackle problems in this engineering domain, DNA nanotechnology has provided some proven solutions,¹⁰ namely by way of bottom-up self-assembly using DNA as a construction material. Progress in this field has largely occurred on two fronts. The first, and original, motivation is to engineer structurally intricate yet stable molecular assemblies at the nanoscale using DNA.¹¹ This is accomplished by programming strands to bind specifically through Watson-Crick base pair-

ing to form rigid multiway branches, which in turn self-assemble into higher-order structures. Prominent examples from an extensive library include 1D,¹²⁻¹⁴ 2D,¹⁵⁻¹⁹ and 3D²⁰⁻²³ tile-based complexes and crystals, and elaborate origami structures²⁴⁻²⁷. Some of these DNA tiles have also served as molecular computing elements.²⁸⁻³⁰

The other impetus behind DNA nanotechnology has been the desire to create dynamic systems, in which DNA assemblies no longer remain static but change their form, carry out functions, or both. Examples of this type include autonomous walkers,³¹⁻³³ molecular motors and robots,³⁴⁻³⁹ and self-replicators⁴⁰. The central mechanism underlying a large portion of these works is toehold-mediated strand displacement reactions,^{41,42} where an invading DNA strand latches onto a short single-stranded toehold domain of a partially double-stranded DNA molecule and undergoes branch migration, displacing one or more of the incumbent strands which can further participate in downstream reactions. Strand displacement reactions have been used to kinetically control DNA self-assembly pathways which has laid the foundations of a major research theme enabling the construction of complex DNA circuits such as cascaded digital^{43,44} and analog⁴⁵ DNA circuits, a chemical reaction network (CRN) to DNA compiler which mimics arbitrary CRN dynamics,⁴⁶ molecular neural networks,⁴⁷ and molecular signal amplifiers⁴⁸.

Recently, there has been some focus, both theoretical^{49,50} and experimental⁵¹⁻⁵³, to integrate the structural and dynamic paradigms of DNA nanotechnology. These experimental works typically consist of a two-part scheme in which an upstream DNA strand displacement circuit interacts with downstream DNA monomers to facilitate isothermal self-assembly. Here, we advance this concept such that an initial DNA structure activates a downstream DNA strand displacement circuit that sequentially leads to polymerization of a new DNA structure, *i.e.*, a DNA structure transfers information *via* non-local DNA strand displacement circuitry to kinetically trans-assemble a new DNA structure (initial DNA structure \rightarrow DNA strand displacement circuitry \rightarrow new DNA structure). We define trans-assembly to be a type of self-assembly in which information embedded in one structure is released and prop-

agated through information-relaying media, ultimately triggering the self-assembly of another structure. This can be conceptually compared to an information-encoded DNA sequence transferring its information to RNA which mediates the creation of gene products. Specifically, an initiator strand is introduced into a system which undergoes toehold-mediated strand displacement with an existing structure to release a single-stranded signal molecule which triggers one of two DNA circuits. Depending on which circuit is triggered, another single-stranded activator molecule is released which binds with a specific type of (inactive) monomer and initiates strand displacement to render the monomers active. The activated monomers then polymerize downstream into a new higher-order DNA nanostructure. Since our system produces only one type of signal strand (per scheme), the final output structure is limited to periodic structures which, when compared with *in vivo* RNA and DNA machinery, is rather primitive in terms of its computational and constructional abilities.

2 Results

2.1 Schematics.

The schematics of the kinetic trans-assembly of DNA nanostructures we tested in our work are illustrated in Fig. 1 (schemes I-IV). All four schemes consist of an initial structure, a DNA strand displacement circuit, and an output structure. The initial structures we used in this work were double-crossover (DX) lattices made from modified DX tiles¹⁵ and ladder structures made from modified T-motifs¹⁴. There are two types of strand displacement circuits we used in this work, circuit I (used in schemes I and III) and circuit II (used in schemes II and IV). Each of these circuits consists of two subcircuits, subcircuit 1 and 2 (SC1 and SC2) for circuit I and subcircuit 3 and 4 (SC3 and SC4) for circuit II. The final output structure, which depends on which subcircuit of a given circuit is triggered, is either a discrete ring structure consisting of another type of modified T-motif or another type of DX lattice (DX-II) composed of modified DX tiles.

Figure 2 depicts the reaction pathways of

schemes I and II, respectively. In each scheme, the system initially comprises an initial structure, two subcircuits, and two types of incomplete precursor motifs all existing in a single pot. Only the initiator strand, I, is later added to the system to trigger the reaction cascade. In scheme I, the initial structure is a DX lattice (denoted DX-i) made up of 2 sequentially different DX tiles, DX-A and DX-B. The DX-A tile of the DX-i structure is divided into several important functional domains (Fig. 2 a, red delineation). In particular, this tile has one hairpin protruding from each plane of the tile, one closed and one open. The open hairpins of the DX-A tiles have a single-stranded toehold domain, t1* (Fig. 2 a, boxed in orange), two consecutive branch migration domains, C and t2 [henceforth, all consecutive functional domains or strands will be denoted as their labels conjoined with hyphens going in the 5' → 3' direction, *e.g.* C-t2, and toehold (sticky-end) domains start with a lowercase 't' ('s')], and single-stranded DX1-s5 domains. Once an initiator strand, I (t1-C), is introduced into the system, it binds at the t1* toehold domain and undergoes strand displacement to displace the incumbent S1 signal strand (C-t2-DX1-s5). The displaced C-t2-DX1-s5 strand acts as a signal to trigger circuit I. The two subcircuits of circuit I, SC1 and SC2, both offer a common single-stranded toehold region t2*, to which the t2 domain of the signal strand can bind. The double-stranded domains following the t2* toehold is different for SC1 and SC2 (DX1* and Tm1*, respectively), meaning branch migration can only proceed along the component which is complementary to the DX1 domain of the signal strand, *i.e.* the SC1 component of circuit I is triggered and the A1 activator strand (DX1-s5-t3-s12-t4-Tm2) is released. Although two types of incomplete precursor motifs (precursor T-motifs and DX tiles) exist in the system, the released A1 activator strand only interacts with pre-annealed incomplete precursor T-motifs through the t3 and t4 toehold domains. Without the activator strand, the precursor T-motif tiles cannot by themselves self-assemble into any specific higher-order structure due to a missing s12 sticky-end. Instead, this missing sticky-end is present in one of the domains of the A1 activator strand, and is provided to the precursor T-motif by way of another strand displacement reaction. The activator strand has a t3-s12-t4 region where t3 and t4

bind to their respective toeholds of the precursor tile and the s12 domain remains single-stranded to fulfill its role as the missing sticky-end. The rest of the activator strand, *i.e.* domain Tm2, displaces the TmP protector strand from the precursor tile to add structural integrity and completes the formation of the T-motif to render it active for self-assembly. The vertical duplexes of the activated T-motifs (Fig. 2 a, yellow delineation) differ in length where the shorter of the two duplexes has a length of 6 nt and the longer duplex has a length of 16 nt (both excluding the sticky-ends). This difference in length leads to an overall curvature so that when these motifs self-assemble, they form a ring structure as designed.

Starting from the same initial DX lattice structure, a different output structure can be obtained by changing the DNA circuit (Fig. 2 b). In scheme II, the reaction profile up to the release of the S1 signal strand is the same as scheme I. The circuit used here, namely circuit II, has two subcircuits, SC3 and SC4. Again, only one of these, SC3, is triggered and strand displacement commences along the DX1* domain. This reaction produces the DX1-s5-t3-DX2-s6 activator strand (A3 strand). In this scheme, the incomplete precursor tiles which interact with the A3 activator strands are of the DX-type with two missing sticky-ends (s5 and s6). The A3 activator strand possessing these missing sticky-end domains first latches onto the t3* toehold region and displaces that DXP protector strand to complete the DX tile (DX-C tile) and activate it for downstream polymerization with DX-D tiles to produce DX-II lattices.

The reaction pathways of the other two schemes are shown in Fig. 3 a and b. In these schemes the initial DNA structures are 1D ladder structures and the output structures are either DX-II lattices (scheme III) or ring structures (scheme IV). The reactions proceed similarly to schemes I and II described above. The initiator strand, I (t1-C), is inserted into the system which displaces the S2 (C-t2-Tm1-s5) signal strand from the initial structure. This signal strand triggers either the SC2 (SC4) strand displacement subcircuit and produces the A2 (A4) activator strand. The A2 (A4) activator strand then binds with the incomplete precursor DX-C tile (T-motif) to activate it for downstream polymerization leading to DX-II (ring) structures.

2.2 Characterization.

Characterizations of our schemes were mainly done by atomic force microscopy (AFM) and agarose gel electrophoresis. Figure 4 shows AFM data of the initial structures and output structures after the strand displacement circuitry reactions have taken place for each of the four schemes (Fig. 4 a-d, respectively). The DX-I lattices (top row of Fig. 4 a, b) and initial ladder structures (top row of Fig. 4 c, d) and can be clearly seen. The bright stripes of the initial DX-I lattices are columns of hairpins which have a measured distance of ~27 nm between each column closely matching the designed distance of ~25 nm (Fig. 5 a, inset). AFM images of the final output structures after the systems have gone through the DNA circuitry are shown on the bottom row of Fig. 4. For the output structure of scheme I, discrete ring structures can be easily imaged along with the remaining DX-I lattices whose signal strands have been displaced by the initiator strands (Fig. 4 a, bottom row). For schemes II-III, the output structures are hairpin-less DX-II lattices (dashed yellow box in the bottom row of Fig. 4 b, c). In scheme IV, initial ladder structures formed from one type of T-motif are trans-assembled into another type of T-motif which self-assemble into ring structures (bottom row of Fig. 4 d). AFM analysis of the average sizes of all 4 initial and output structures is shown in Figure S7.

3 Discussion

Some important points concerning our experiments are worth mentioning.

3.1 Yield.

One of the determining factors of the final yield of the output structures is in how well the initial structures form. The initial DX-I and ladder structures we designed were assembled from modified DX tiles and T-motifs, respectively, yet their yields and lattice sizes were comparable to their original unmodified counterparts.^{14,18} These initial structures were then purified by spin filtration before use in our experiments (see Methods). AFM images of only the annealed DX-I and ladder lattices

after spin filtration without any other elements or DNA circuitry in the system show well-formed initial structures (Fig. 5 a, b and Supplementary Fig. 6). Another factor which may be important in the yield of the output structures is the number of reaction layers the information needs to proceed through in order to produce the final products. This factor may play a role in reducing the yields of the output structures in our schemes compared with previously reported schemes with fewer reaction layers⁵¹⁻⁵³.

3.2 Prevention of leak reactions.

Another important point to consider when using DNA strand displacement circuitry is dealing with leak reactions,^{42,45} *i.e.* spurious strand displacement events bypassing the intended reaction pathway and leading to unwanted signal production. Several preventive measures were taken to minimize leak reactions. First, the initial structures were purified by spin filtration before being used in the experiments to remove any single strands remaining in the system, especially any unattached signal strands (strands which are not part of the initial structure; see Methods and Supplementary Fig. 6). All data were obtained using these purified initial structures. As another preventive measure, the DNA subcircuits and other extant motifs in the system (SC1-4, incomplete precursor T-motifs and DX-C tiles, and complete DX-D tiles) were purified before use in order to minimize leak reactions coming from these elements. Each of the four subcircuits were annealed and run under a 2% agarose gel (Fig. 5 c). After confirming clear and discrete bands for all four subcircuits, the bands were extracted and purified using a Freeze N Squeeze spin column (see Methods). In this way, unhybridized residues were minimized, especially unhybridized activator strands, while simultaneously maximizing the use of well-formed ones. This double preventive strategy seems to be effective since if there were any significant amount of leak reactions, then observation of the final output structures should be possible without the introduction of the initiator strand. In other words, at least some output structures should have been observed in the AFM images before the inclusion of the initiator strand (Fig. 4 top row). The fact that not a single output structure, either DX-II lattices

or rings, was observed in the analysis of over 50 images for each scheme before the addition of the initiator strand strongly suggests the robustness of our DNA strand displacement scheme. Furthermore, this holds true even in samples which were imaged after ~ 7 days of storage at 4°C . Only by adding the initiator strand to the system do the reactions proceed according to design and is the final output structure produced.

Another potential source of leakage reactions comes from the possibility of the wrong subcircuit of the DNA circuit being triggered. For example in scheme I, only the SC1 subcircuit of circuit I is designed to be triggered to release the A1 activator strand but the possibility of the SC2 subcircuit releasing the A2 activator strand (Tm1-s5-t3-DX2-s6) exists. This may happen either by spontaneous dissociation of the A2 activator strand from SC2 or effectively due to any single-stranded A2 residues in the system. We do not believe this to be the case since leakage of A2 activator strands would provide the missing sticky-ends to the incomplete precursor DX-C tiles and make them active which in turn would enable bindings with extant DX-D tiles leading to the self-assembly of DX-II lattices. As can be seen in Fig. 4 a (bottom image), no DX-II lattices were observed (in over 50 AFM images) suggesting negligible production of A2, if any. The same can be said for schemes II, III, and IV; only the intended activator strand becomes released and insignificant amounts of leakage occurs for all subcircuits of a given circuit.

3.3 Control data of the output structures.

Figure 5 d-g shows control data of the output structures (see Methods). These structures were individually annealed without any other elements, *e.g.* DNA circuits, and did not go through the strand displacement reaction process. Figures 5 d and 5 e show AFM data of samples annealed with the two types of tiles making up DX-II structures without and with the A3 activator strand, respectively. Without the A3 strand, only small lattice fragments can be seen (the AFM data shown in Fig. 5 d used samples with concentrations over $\times 13$ the ones used in our experiments to emphasize the formation of unintended lattice fragments,

see Supplementary Fig. 8) whereas samples annealed with the A3 strand included show fully formed DX-II lattices. Figure 5 f shows that annealing the incomplete precursor T-motifs by themselves cannot produce rings, but do produce rings when annealed with the A1 activator strands (Fig. 5 g).

4 Conclusion

Controlled propagation of information emanating from one entity to ultimately activate or create another entity is ubiquitous in natural and synthetic biology. Whether it be receptor proteins interacting with a gene regulatory network for gene expression, membrane receptors binding with primary messengers to trigger signal transduction cascades leading to cellular responses, or activated promoters going through synthetic biological circuits leading to a desired gene product, control of information flow underlies the crucial metabolic processes of the cell. In this regard, the trans-assembly of an output structure from an initial structure *via* DNA strand displacement circuitry we have shown here offers a purely DNA analogue of the aforementioned biological processes in the context of DNA nanotechnology. The two major paradigms of DNA nanotechnology, namely the structural self-assembly of DNA nanostructures and the dynamic transfer of information have been combined into a single system to provide an isothermal self-assembly platform. Furthermore, this method can be readily generalized and is not relegated to certain structures or circuits. Although the experiments in this work were conducted under a single set of conditions (*e.g.* temperature, salinity, *etc.*), given the robustness of both the DNA strand displacement reactions^{45,54} and DNA self-assembly, the main results presented here seem likely to hold for a range of temperatures and conditions. Additionally, none of the strand sequences for both the motifs and, more importantly, the DNA circuits were optimized (except checking for repeating segments)⁵⁵, providing further support for this assumption.

On a more fundamental level, one may ask whether these types of integrated systems offer any advantages over implementing DNA tile assembly or DNA strand displacement circuitry sys-

tems separately. It is known that DNA tile assembly in 2D and 3D is Turing-universal⁵⁶ which allows for the self-assembly of arbitrary shapes from small tile sets⁵⁷. As for CRNs, arbitrary CRN dynamics can be systematically implemented using the formal language of DNA strand displacement circuitry⁴⁶. Recent theoretical works^{49,50} give some insight into what is theoretically possible by integrating these two paradigms. For example, the proposed minimal model in Ref. 49 incorporates the non-local nature of CRNs to influence the local assembly logic of tile assembly, and *vice versa*. This model is shown to be efficiently Turing-universal even in (unbounded) 1D. Moreover, arbitrary shapes can be produced using programs created within this formalism with the program complexity bounded by the Kolmogorov complexity of the shape, without the sometimes large scale factor required for programs created within the framework of the abstract tile assembly model⁵⁷. The same authors extend these results in Ref. 50 to show that, in addition to the previously reported space and program size complexity efficiency,⁴⁹ the efficiency of computational and construction time complexity of the minimal model is at least as good if not better than either system alone.

Open questions remain as to what can be fully accomplished by integrating these two molecular programming paradigms. Perhaps the most far-reaching is, "How much of the parallel nature of (DNA) molecular computing can these systems harness?" A new theoretical model or framework may be needed to answer this question since both of the theoretical works mentioned above enforce sequential computation/construction.^{49,50} Even finding physical DNA tile implementations of the minimal model proposed in Ref. 49 may prove difficult since the abstract tile assembly model is grounded on different presumptions⁵⁸. Experimental studies based on a different type of strand displacement mechanism, namely hybridization chain reaction, may serve as a guide in answering these questions^{53,59-62} but unfortunately a broad theoretical framework is currently lacking. Although much still needs to be done, the multilayer, multiple circuit approach of this study to integrate dynamic information propagation with the self-assembly of DNA nanostructures shows that the two different DNA chemistries can be carefully coordinated to mimic the rich and di-

verse realm of natural biochemical systems.

5 Materials and Methods

5.1 DNA oligo synthesis

Synthetic oligonucleotides were purchased from Bioneer (Daejeon, Korea) and purified by polyacrylamide gel electrophoresis (PAGE). The details can be found at www.bioneer.co.kr. The details of the strand sequences can be found in the supplementary information.

5.2 Annealing protocol of complexes

All the complexes used in schemes I-IV were self-assembled by mixing stoichiometric quantities of each strand in a physiological buffer, 1×TAE/Mg²⁺ [Tris-Acetate-EDTA (40 mM Tris, 1 mM EDTA, pH 8.0) with 12.5 mM magnesium acetate]. Each of the complexes [the initial ladder structures, initial DX-I lattices, each subcircuit (SC1-4), incomplete precursor T-motifs, incomplete precursor DX-C tiles, and complete DX-D tiles] were separately annealed from 95 °C to 25 °C by placing the solution-filled microtubes in 1.5 L of boiled water in a styrofoam box for at least 24 hours to facilitate hybridization. The final complex/tile/motif concentrations were 2 μM. For the control samples used in Fig. 5 d-g, each sample was separately prepared in a one-pot annealing procedure at a tile/motif concentration of 400 nM.

5.3 Purification of complexes

All the complexes obtained by annealing were purified by either agarose gel electrophoresis or spin filtration. Each of the 2 μM samples of the discrete complexes obtained by annealing (*i.e.* SC1-4, incomplete precursor T-motifs, incomplete precursor DX-C tiles, and complete DX-D tiles) were run under a 2% agarose gel and 1×TAE/Mg²⁺ running buffer solution at 60 V for 2 hours. After the run, the gel was stained with SYBR Gold (Thermo Fisher Scientific, Massachusetts, USA) and imaged with a Molecular Imager Gel Doc XR system (Bio-Rad, California, USA). To extract gel bands, the gel was placed under a High Performance 2UV Transilluminator (UVP, Jena, Ger-

many), excised with a gel cutter, and put into a Freeze N Squeeze microtube (Bio-Rad, California, USA). The microtube was put in a -20°C freezer for 5 min, then removed and immediately centrifuged at $13,000 \times \text{r.c.f.}$ (relative centrifugal force) for 3 min at room temperature. The DNA concentration of extracted structures was measured by Nanodrop 2000 (Thermo Fisher Scientific, Massachusetts, USA). The $2 \mu\text{M}$ initial (non-discrete) structures, *i.e.* ladder and DX-I lattices, were diluted to 800 nM and purified using a 100kDa molecular weight cut-off (MWCO) Amicon centrifugal filter (Sigma-Aldrich, St. Louis, Missouri, USA). $100 \mu\text{L}$ of the 800 nM samples and an additional $400 \mu\text{L}$ of $1 \times \text{TAE}/\text{Mg}^{2+}$ buffer solution were added into the filter. After spinning for 3 min at $3,000 \times \text{r.c.f.}$, another $400 \mu\text{L}$ of $1 \times \text{TAE}/\text{Mg}^{2+}$ buffer was added for a second wash and repeated three times. The DNA volume/concentration of the filtered initial structures (ladders and DX-I structures) were typically $\sim 100 \mu\text{L}/100 \text{ nM}$ when measured with the Nanodrop 2000.

5.4 Sample preparation for kinetic trans-assembly

A total of four different schemes (schemes I-IV) were prepared. For each scheme, stoichiometric amounts of the initial DNA structure, two DNA subcircuits (SC1 and SC2 or SC3 and SC4), incomplete precursor T-motifs, incomplete precursor DX tiles, and DX-D tiles were pipetted into a single microtube. To start the reaction cascade, $10 \times$ the amount of the initiator strand (compared to the other components) was pipetted into the microtube. The final concentration of the initiator strand was 300 nM and the final concentration of the rest of the components was 30 nM. The microtubes were kept at 30°C for 4 hours to facilitate the strand displacement and self-assembly reactions. Details of the stoichiometric quantities of each component used in each scheme can be found in the Supporting Information.

5.5 AFM imaging

To obtain the AFM images, $2 \mu\text{L}$ of the samples were placed on freshly cleaved mica for 30 seconds after which $48 \mu\text{L}$ of $1 \times \text{TAE}/\text{Mg}^{2+}$ buffer was

pipetted onto the mica surface. For AFM images of the control experiments in Fig. 5 d-g, $10 \mu\text{L}$ of the samples were placed on freshly cleaved mica for 30 seconds after which $40 \mu\text{L}$ of $1 \times \text{TAE}/\text{Mg}^{2+}$ buffer was pipetted onto the mica surface. AFM images were taken by 3 different instruments. A NanoWizard ULTRASPEED AFM (JPK Instruments, Berlin, Germany) in Fast imaging mode under a buffer using a wear resistant high density carbon/diamond like carbon (HDC/DLC) USC-F0.3-k0.3-10 tips (NanoWorld, Neuchâtel, Switzerland), Digital Instruments Nanoscope III (Veeco Inc., New York, USA) in tapping mode under a buffer using DNP-S10 silicon nitride tips (Bruker, Massachusetts, USA), and MFP-3D-BIO (Asylum Research, California, USA) in liquid AC mode under a buffer using DNP-S10 silicon nitride tips (Bruker, Massachusetts, USA).

6 Acknowledgements

This research was supported by grants from the Korea Research Institute of Bioscience and Biotechnology (KRIBB) Research Initiative Program and the R&D Convergence Program (CAP-14-3-KRISS).

7 Author Contributions

J.S. and J.K. conceived and directed the project and designed the experiments, J.S. conducted the experiments, J.S., J.K., T.H.H., and S.H.P. analysed the data, J.K. and J.S. wrote the paper, and T.H.H. supervised the project. All authors commented on the manuscript.

8 Associated Content

The Supporting Information includes the DNA sequence details and additional AFM images.

References

- [1] David L. Nelson and Michael M. Cox. *Lehninger Principles of Biochemistry, 5e.* W H. Freeman and Company, 2008. ISBN 0-7167-7r08-X.

- [2] Erin D. Goley and Matthew D. Welch. The Arp2/3 Complex: an Actin Nucleator Comes of Age. *Nat. Rev. Mol. Cell Biol.*, 7(10):713–726, 2006. doi: 10.1038/nrm2026. URL <https://doi.org/10.1038/nrm2026>.
- [3] Seyun Kim and Pierre A. Coulombe. Emerging Role for the Cytoskeleton As an Organizer and Regulator of Translation. *Nat. Rev. Mol. Cell Biol.*, 11(1):75–81, 2010. doi: 10.1038/nrm2818. URL <https://doi.org/10.1038/nrm2818>.
- [4] Gary J. Brouhard and Luke M. Rice. Microtubule dynamics: an interplay of biochemistry and mechanics. *Nat. Rev. Mol. Cell Biol.*, 2018. doi: 10.1038/s41580-018-0009-y. URL <https://doi.org/10.1038/s41580-018-0009-y>.
- [5] Lisa A. Cameron, Paula A. Giardini, Frederick S. Soo, and Julie A. Theriot. Secrets of actin-based motility revealed by a bacterial pathogen. *Nat. Rev. Mol. Cell Biol.*, 1:110–119, 2000. doi: 10.1038/35040061. URL <https://dx.doi.org/10.1038/35040061>.
- [6] Céline Revenu, Rafika Athman, Sylvie Robine, and Daniel Louvard. The Co-Workers of Actin Filaments: From Cell Structures To Signals. *Nat. Rev. Mol. Cell Biol.*, 5(8):635–646, 2004. doi: 10.1038/nrm1437. URL <https://doi.org/10.1038/nrm1437>.
- [7] Carsten Janke and Jeannette Chloë Bulinski. Post-Translational Regulation of the Microtubule Cytoskeleton: Mechanisms and Functions. *Nat. Rev. Mol. Cell Biol.*, 12(12):773–786, 2011. doi: 10.1038/nrm3227. URL <https://doi.org/10.1038/nrm3227>.
- [8] Anna Akhmanova and Michel O. Steinmetz. Control of Microtubule Organization and Dynamics: Two Ends in the Limelight. *Nat. Rev. Mol. Cell Biol.*, 16(12):711–726, 2015. doi: 10.1038/nrm4084. URL <https://doi.org/10.1038/nrm4084>.
- [9] Kerry Bloom and Ajit Joglekar. Towards Building a Chromosome Segregation Machine. *Nature*, 463(7280):446–456, 2010. doi: 10.1038/nature08912. URL <https://doi.org/10.1038/nature08912>.
- [10] Wolfgang Pfeifer and Barbara Saccà. Synthetic DNA Filaments: From Design To Applications. *Biol. Chem.*, 2018. doi: 10.1515/hsz-2018-0110. URL <https://doi.org/10.1515/hsz-2018-0110>.
- [11] Fei Zhang, Jeanette Nangreave, Yan Liu, and Hao Yan. Structural DNA Nanotechnology: State of the Art and Future Perspective. *J. Am. Chem. Soc.*, 136(32):11198–11211, 2014. doi: 10.1021/ja505101a. URL <https://doi.org/10.1021/ja505101a>.
- [12] Dage Liu, Sung Ha Park, John H. Reif, and Thomas H. LaBean. DNA Nanotubes Self-Assembled From Triple-Crossover Tiles As Templates for Conductive Nanowires. *Proc. Natl. Acad. Sci. U. S. A.*, 101(3):717–722, 2004. doi: 10.1073/pnas.0305860101. URL <https://doi.org/10.1073/pnas.0305860101>.
- [13] Peng Yin, Rizal F. Hariadi, Sudheer Sahu, Harry M. T. Choi, Sung Ha Park, Thomas H. LaBean, and John H. Reif. Programming DNA Tube Circumferences. *Science*, 321(5890):824–826, 2008. doi: 10.1126/science.1157312. URL <https://doi.org/10.1126/science.1157312>.
- [14] Shogo Hamada and Satoshi Murata. Substrate-Assisted Assembly of Interconnected Single-Duplex DNA Nanostructures. *Angew. Chem., Int. Ed.*, 121(37):6952–6955, 2009. doi: 10.1002/ange.200902662. URL <https://doi.org/10.1002/ange.200902662>.
- [15] Erik Winfree, Furong Liu, Lisa A. Wenzler, and Nadrian C. Seeman. Design and Self-Assembly of Two-Dimensional DNA Crystals. *Nature*, 394(6693):539–544, 1998. doi: 10.1038/28998. URL <https://doi.org/10.1038/28998>.
- [16] Hao Yan, Sung Ha Park, Gleb Finkelstein, John H. Reif, and Thomas H. LaBean. DNA-Templated Self-Assembly of Protein Arrays and Highly Conductive Nanowires. *Science*, 301(5641):1882, 2003. doi: 10.1126/science.1089389.

- URL <http://www.sciencemag.org/content/301/5641/1882.abstract>.
- [17] Yu He, Yi Chen, Haipeng Liu, Alexander E. Ribbe, and Chengde Mao. Self-Assembly of Hexagonal DNA Two-Dimensional (2D) Arrays. *J. Am. Chem. Soc.*, 127(35): 12202, 2005. doi: 10.1021/ja0541938. URL <http://pubs.acs.org/doi/abs/10.1021/ja0541938>.
- [18] Jihoon Shin, Junghoon Kim, Rashid Amin, Seungjae Kim, Young Hun Kwon, and Sung Ha Park. Artificial DNA Lattice Fabrication By Noncomplementarity and Geometrical Incompatibility. *ACS Nano*, 5(6):5175–5179, 2011. doi: 10.1021/nn201312g. URL <https://doi.org/10.1021/nn201312g>.
- [19] Bryan Wei, Mingjie Dai, and Peng Yin. Complex Shapes Self-Assembled From Single-Stranded DNA Tiles. *Nature*, 485(7400):623–626, 2012. doi: 10.1038/nature11075. URL <https://doi.org/10.1038/nature11075>.
- [20] Jianping Zheng, Jens J. Birktoft, Yi Chen, Tong Wang, Ruojie Sha, Pamela E. Constantinou, Stephan L. Ginell, Chengde Mao, and Nadrian C. Seeman. From Molecular To Macroscopic Via the Rational Design of a Self-Assembled 3d DNA Crystal. *Nature*, 461(7260):74–77, 2009. doi: 10.1038/nature08274. URL <https://doi.org/10.1038/nature08274>.
- [21] Yonggang Ke, Luvena L. Ong, William M. Shih, and Peng Yin. Three-Dimensional Structures Self-Assembled from DNA Bricks. *Science*, 338(6111):1177–1183, 2012. doi: 10.1126/science.1227268. URL <http://www.sciencemag.org/content/338/6111/1177.abstract>.
- [22] Yonggang Ke, Luvena L. Ong, Wei Sun, Jie Song, Mingdong Dong, William M. Shih, and Peng Yin. DNA Brick Crystals With Prescribed Depths. *Nat. Chem.*, 6(11):994–1002, 2014. doi: 10.1038/nchem.2083. URL <https://doi.org/10.1038/nchem.2083>.
- [23] Luvena L. Ong, Nikita Hanikel, Omar K. Yaghi, Casey Grun, Maximilian T. Strauss, Patrick Bron, Josephine Lai-Kee-Him, Florian Schueder, Bei Wang, Pengfei Wang, Jocelyn Y. Kishi, Cameron Myhrvold, Allen Zhu, Ralf Jungmann, Gaetan Bellot, Yonggang Ke, and Peng Yin. Programmable self-assembly of three-dimensional nanostructures from 10,000 unique components. *Nature*, 552(7683):72–77, 2017. doi: 10.1038/nature24648. URL <https://doi.org/10.1038/nature24648>.
- [24] Paul W. K. Rothemund. Folding DNA To Create Nanoscale Shapes and Patterns. *Nature*, 440(7082):297–302, 2006. doi: 10.1038/nature04586. URL <https://doi.org/10.1038/nature04586>.
- [25] Dongran Han, Suchetan Pal, Jeanette Nangreave, Zhengtao Deng, Yan Liu, and Hao Yan. DNA Origami with Complex Curvatures in Three-Dimensional Space. *Science*, 332(6027): 342, 2011. doi: 10.1126/science.1202998. URL <http://www.sciencemag.org/content/332/6027/342.abstract>.
- [26] Grigory Tikhomirov, Philip Petersen, and Lulu Qian. Fractal Assembly of Micrometre-Scale DNA Origami Arrays With Arbitrary Patterns. *Nature*, 552(7683):67–71, 2017. doi: 10.1038/nature24655. URL <https://doi.org/10.1038/nature24655>.
- [27] Klaus F. Wagenbauer, Christian Sigl, and Hendrik Dietz. Gigadalton-Scale Shape-Programmable DNA Assemblies. *Nature*, 552(7683):78–83, 2017. doi: 10.1038/nature24651. URL <https://doi.org/10.1038/nature24651>.
- [28] Chengde Mao, Thomas H. LaBean, John H. Reif, and Nadrian C. Seeman. Logical computation using algorithmic self-assembly of DNA triple-crossover molecules. *Nature*, 407:493–496, 2000. doi: 10.1038/35035038. URL <https://dx.doi.org/10.1038/35035038>.
- [29] Paul W. K Rothemund, Nick Papadakis, and Erik Winfree. Algorithmic Self-Assembly

- of DNA Sierpinski Triangles. *PLoS Biology*, 2(12):e424, 2004. doi: 10.1371/journal.pbio.0020424. URL <https://doi.org/10.1371/journal.pbio.0020424>.
- [30] Junghoon Kim, Tai Hwan Ha, and Sung Ha Park. Substrate-Assisted 2D DNA Lattices and Algorithmic Lattices From Single-Stranded Tiles. *Nanoscale*, 7(29):12336–12342, 2015. doi: 10.1039/c5nr03088a. URL <https://doi.org/10.1039/c5nr03088a>.
- [31] Jonathan Bath, Simon J. Green, and Andrew J. Turberfield. A Free-Running DNA Motor Powered By a Nicking Enzyme. *Angew. Chem., Int. Ed.*, 44(28):4358–4361, 2005. doi: 10.1002/anie.200501262. URL <https://doi.org/10.1002/anie.200501262>.
- [32] Ye Tian, Yu He, Yi Chen, Peng Yin, and Chengde Mao. A DNAzyme That Walks Processively and Autonomously Along a One-Dimensional Track. *Angew. Chem., Int. Ed.*, 44(28):4355–4358, 2005. doi: 10.1002/anie.200500703. URL <https://doi.org/10.1002/anie.200500703>.
- [33] Peng Yin, Harry M. T. Choi, Colby R. Calvert, and Niles A. Pierce. Programming Biomolecular Self-Assembly Pathways. *Nature*, 451(7176):318–322, 2008. doi: 10.1038/nature06451. URL <https://doi.org/10.1038/nature06451>.
- [34] Tosan Omabegho, Ruojie Sha, and Nadrian C. Seeman. A Bipedal DNA Brownian Motor With Coordinated Legs. *Science*, 324(5923):67–71, 2009. doi: 10.1126/science.1170336. URL <https://doi.org/10.1126/science.1170336>.
- [35] Kyle Lund, Anthony J. Manzo, Nadine Dabby, Nicole Michelotti, Alexander Johnson-Buck, Jeanette Nangreave, Steven Taylor, Renjun Pei, Milan N. Stojanovic, Nils G. Walter, Erik Winfree, and Hao Yan. Molecular robots guided by prescriptive landscapes. *Nature*, 465:206–210, 2010. doi: doi:10.1038/nature09012. URL <http://dx.doi.org/10.1038/nature09012>.
- [36] Shelley F. J. Wickham, Masayuki Endo, Yousuke Katsuda, Kumi Hidaka, Jonathan Bath, Hiroshi Sugiyama, and Andrew J. Turberfield. Direct Observation of Stepwise Movement of a Synthetic Molecular Transporter. *Nat. Nanotechnol.*, 6(3):166–169, 2011. doi: 10.1038/nnano.2010.284. URL <https://doi.org/10.1038/nnano.2010.284>.
- [37] Richard A. Muscat, Jonathan Bath, and Andrew J. Turberfield. A Programmable Molecular Robot, 2011. URL <http://dx.doi.org/10.1021/nl1037165>. PMID: 21275404.
- [38] Shawn M. Douglas, Ido Bachelet, and George M. Church. A Logic-Gated Nanorobot for Targeted Transport of Molecular Payloads. *Science*, 335(6070):831–834, 2012. ISSN 0036-8075. doi: 10.1126/science.1214081. URL <http://science.sciencemag.org/content/335/6070/831>.
- [39] Anupama J. Thubagere, Wei Li, Robert F. Johnson, Zibo Chen, Shayan Doroudi, Yae Lim Lee, Gregory Izatt, Sarah Wittman, Niranjan Srinivas, Damien Woods, Erik Winfree, and Lulu Qian. A Cargo-Sorting DNA Robot. *Science*, 357(6356):eaan6558, 2017. doi: 10.1126/science.aan6558. URL <https://doi.org/10.1126/science.aan6558>.
- [40] Junghoon Kim, Junwye Lee, Shogo Hamada, Satoshi Murata, and Sung Ha Park. Self-replication of DNA rings. *Nat. Nanotechnol.*, 10(6):528–533, 2015. doi: 10.1038/nnano.2015.87. URL <https://doi.org/10.1038/nnano.2015.87>.
- [41] Bernard Yurke, Andrew J. Turberfield, Allen P. Mills, Friedrich C. Simmel, and Jennifer L. Neumann. A DNA-Fuelled Molecular Machine Made of DNA. *Nature*, 406(6796):605–608, 2000. doi: 10.1038/35020524. URL <https://doi.org/10.1038/35020524>.
- [42] David Yu Zhang and Georg Seelig. Dynamic DNA Nanotechnology Using Strand-Displacement Reactions. *Nat. Chem.*, 3(2):103–113, 2011. doi: 10.1038/nchem.957. URL <https://doi.org/10.1038/nchem.957>.

- [43] Georg Seelig, David Soloveichik, David Yu Zhang, and Erik Winfree. Enzyme-Free Nucleic Acid Logic Circuits. *Science*, 314(5805):1585–1588, 2006. doi: 10.1126/science.1132493. URL <https://doi.org/10.1126/science.1132493>.
- [44] Lulu Qian and Erik Winfree. Scaling Up Digital Circuit Computation With DNA Strand Displacement Cascades. *Science*, 332(6034):1196–1201, 2011. doi: 10.1126/science.1200520. URL <https://doi.org/10.1126/science.1200520>.
- [45] David Yu Zhang, Andrew J. Turberfield, Bernard Yurke, and Erik Winfree. Engineering Entropy-Driven Reactions and Networks Catalyzed By DNA. *Science*, 318(5853):1121–1125, 2007. doi: 10.1126/science.1148532. URL <https://doi.org/10.1126/science.1148532>.
- [46] Niranjan Srinivas, James Parkin, Georg Seelig, Erik Winfree, and David Soloveichik. Enzyme-free nucleic acid dynamical systems. *Science*, 358(6369), 2017. ISSN 0036-8075. doi: 10.1126/science.aal2052. URL <http://science.sciencemag.org/content/358/6369/eaal2052>.
- [47] Lulu Qian, Erik Winfree, and Jehoshua Bruck. Neural Network Computation With DNA Strand Displacement Cascades. *Nature*, 475(7356):368–372, 2011. doi: 10.1038/nature10262. URL <https://doi.org/10.1038/nature10262>.
- [48] Xi Chen, Neima Briggs, Jeremy R. McLain, and Andrew D. Ellington. Stacking Nonenzymatic Circuits for High Signal Gain. *Proc. Natl. Acad. Sci. U. S. A.*, 110(14):5386–5391, 2013. doi: 10.1073/pnas.1222807110. URL <https://doi.org/10.1073/pnas.1222807110>.
- [49] Nicholas Schiefer and Erik Winfree. *Universal Computation and Optimal Construction in the Chemical Reaction Network-Controlled Tile Assembly Model*, pages 34–54. Springer International Publishing, 2015. ISBN 978-3-319-21999-8. doi: 10.1007/978-3-319-21999-8_3.
- [50] Nicholas Schiefer and Erik Winfree. *Time Complexity of Computation and Construction in the Chemical Reaction Network-Controlled Tile Assembly Model*, pages 165–182. Springer International Publishing, Cham, 2016. ISBN 978-3-319-43994-5. doi: 10.1007/978-3-319-43994-5_11. URL https://doi.org/10.1007/978-3-319-43994-5_11.
- [51] David Yu Zhang, Rizal F. Hariadi, Harry M.T. Choi, and Erik Winfree. Integrating DNA Strand-Displacement Circuitry With DNA Tile Self-Assembly. *Nat. Commun.*, 4(nil):nil, 2013. doi: 10.1038/ncomms2965. URL <https://doi.org/10.1038/ncomms2965>.
- [52] Dongbao Yao, Tingjie Song, Xianbao Sun, Shiyan Xiao, Fujian Huang, and Haojun Liang. Integrating DNA-Strand-Displacement Circuitry With Self-Assembly of Spherical Nucleic Acids. *J. Am. Chem. Soc.*, 137(44):14107–14113, 2015. doi: 10.1021/jacs.5b07453. URL <https://doi.org/10.1021/jacs.5b07453>.
- [53] Zhuo Zhang, Tsz Wing Fan, and I-Ming Hsing. Integrating DNA Strand Displacement Circuitry To the Nonlinear Hybridization Chain Reaction. *Nanoscale*, 9(8):2748–2754, 2017. doi: 10.1039/c6nr06589a. URL <https://doi.org/10.1039/c6nr06589a>.
- [54] David Yu Zhang, Sherry Xi Chen, and Peng Yin. Optimizing the Specificity of Nucleic Acid Hybridization. *Nat. Chem.*, 4(3):208–214, 2012. doi: 10.1038/nchem.1246. URL <https://doi.org/10.1038/nchem.1246>.
- [55] Junghoon Kim. SEQMAK: A program for producing DNA sequences. *Zenodo*, 2016. doi: <http://doi.org/10.5281/zenodo.59874>. URL <https://www.github.com/jfkimberly/SEQMAK>.
- [56] Erik Winfree, Xiaoping Yang, and Nadrian C. Seeman. Universal Computation via Self-assembly of DNA: Some Theory and Experiments. In *DNA Based Computers II, volume 44 of DIMACS*, pages 191–213. American Mathematical Society, 1996.

- [57] David Soloveichik and Erik Winfree. Complexity of self-assembled shapes. *SIAM J. Comp.*, 36:1544–1569, 2007.
- [58] E. Winfree. Simulations of computing by self-assembly. *Caltech Technical Report CS-TR:1988.22*, 1998.
- [59] Zhou Nie, Pengfei Wang, Cheng Tian, and Chengde Mao. Synchronization of Two Assembly Processes To Build Responsive DNA Nanostructures. *Angew. Chem., Int. Ed.*, 53(32):8402–8405, 2014. doi: 10.1002/anie.201404307. URL <https://doi.org/10.1002/anie.201404307>.
- [60] Jennifer E. Padilla, Ruojie Sha, Martin Kristiansen, Junghuei Chen, Natasha Jonoska, and Nadrian C. Seeman. A Signal-Passing DNA-Strand-Exchange Mechanism for Active Self-Assembly of DNA Nanostructures. *Angew. Chem., Int. Ed.*, 54(20):5939–5942, 2015. doi: 10.1002/anie.201500252. URL <https://doi.org/10.1002/anie.201500252>.
- [61] Sarah Helmig and Kurt Vesterager Gothelf. AFM Imaging of Hybridization Chain Reaction Mediated Signal Transmission Between Two DNA Origami Structures. *Angew. Chem., Int. Ed.*, 56(44):13633–13636, 2017. doi: 10.1002/anie.201706680. URL <https://doi.org/10.1002/anie.201706680>.
- [62] Gourab Chatterjee, Neil Dalchau, Richard A. Muscat, Andrew Phillips, and Georg Seelig. A Spatially Localized Architecture for Fast and Modular DNA Computing. *Nat. Nanotechnol.*, 12(9):920–927, 2017. doi: 10.1038/nnano.2017.127. URL <https://doi.org/10.1038/nnano.2017.127>.

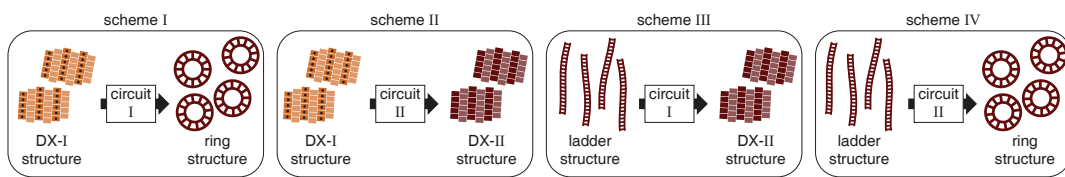


Figure 1: Kinetic trans-assembly of DNA nanostructures through DNA strand displacement circuitry. The four schemes (I-IV) implemented in this work.

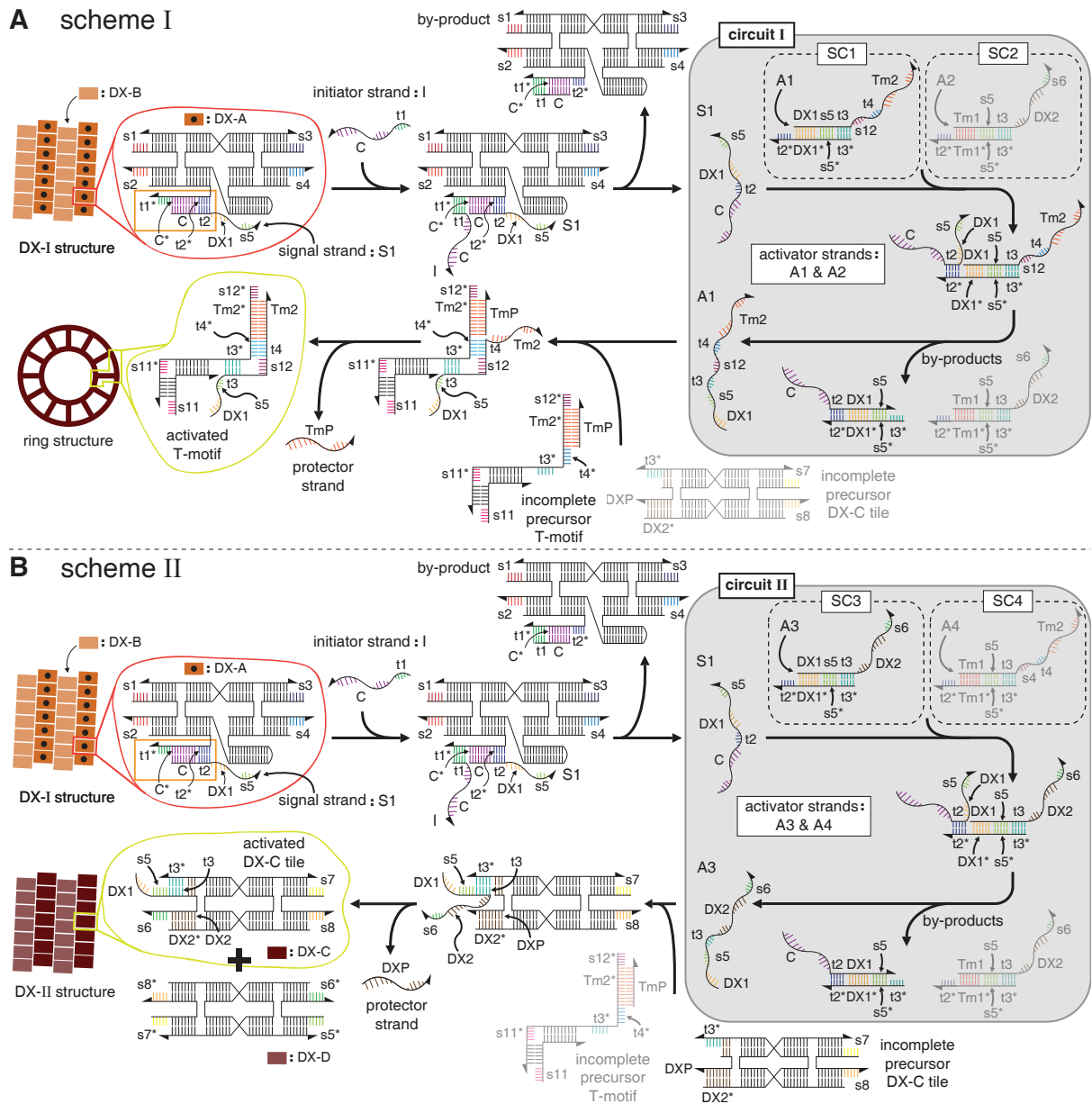
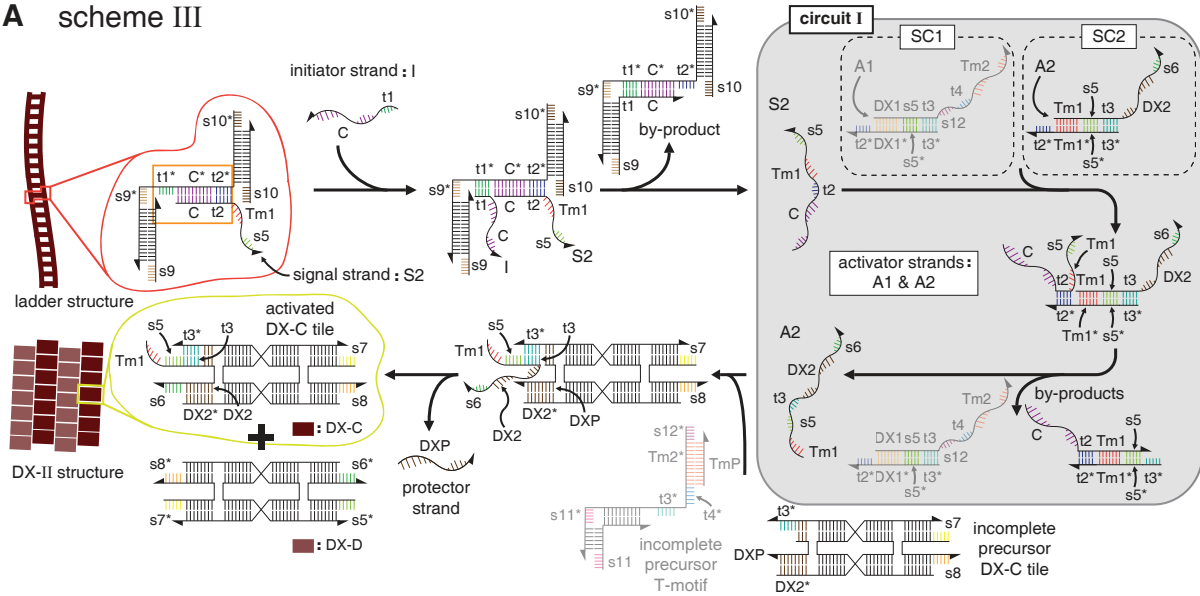


Figure 2: Schematics of schemes I and II. **a** Details of scheme I. The reaction starts with an initial DX-I structure made from DX-A and DX-B tiles. The DX-A tile has an open hairpin region (boxed in orange) which possesses an exposed $t1^*$ toehold domain. When the initiator strand I ($t1$ -C) is inserted into the system, its $t1$ domain hybridizes with the $t1^*$ toehold domain of DX-A, which facilitates branch migration of the C domain to displace the signal strand S1 (C- $t2$ -DX1- $s5$). This signal strand activates circuit I which includes two subcircuits, SC1 and SC2, who share a common toehold $t2^*$ but are otherwise sequentially orthogonal. The $t2$ domain of the signal strand can bind to the $t2^*$ toehold of either SC1 or SC2 but branch migration only occurs for SC1, since it is the only one with a common DX1 branch migration domain. The signal strand for scheme I activates SC1 of circuit I which produces the activator strand A1 (DX1- $s5$ - $t3$ - $s12$ - $t4$ -Tm2). This binds to an incomplete precursor T-motif at the $t3^*$ and $t4^*$ toehold domains. Without the A1 activator strands, these precursor T-motifs cannot self-assemble into higher-order structures due to the missing $s12$ sticky-end. The domain between the $t3$ and $t4$ domains of the invading A1 activator strand provides this missing $s12$ sticky-end. Once bound at these toehold domains, the A1 strand displaces the TmP protector strand to complete the formation of a new T-motif which self-assembles into a ring structure. **b** Details of scheme II. The reaction cascade up to the production of the signal strand S1 is the same as scheme I. The signal strand for scheme II activates SC3 of circuit II which produces the activator strand A3 (DX1- $s5$ - $t3$ -DX2- $s6$) through strand displacement. After binding at the $t3^*$ toehold domain, this A3 activator strand provides the missing $s5$ and $s6$ sticky-ends. The $s6$ sticky-end is provided by displacing the DXP protector strand. This activates the DX-C tile and allows for sticky-end bindings with DX-D tiles to produce DX-II lattices. All functional domains are colour-coded and labeled; their complementary counterparts are starred (e.g. DX1 and DX1*). Half-arrowheads on the strands indicate the 3' direction. Components shown at half opacity stay non-reactive for that particular scheme.

A scheme III



B scheme IV

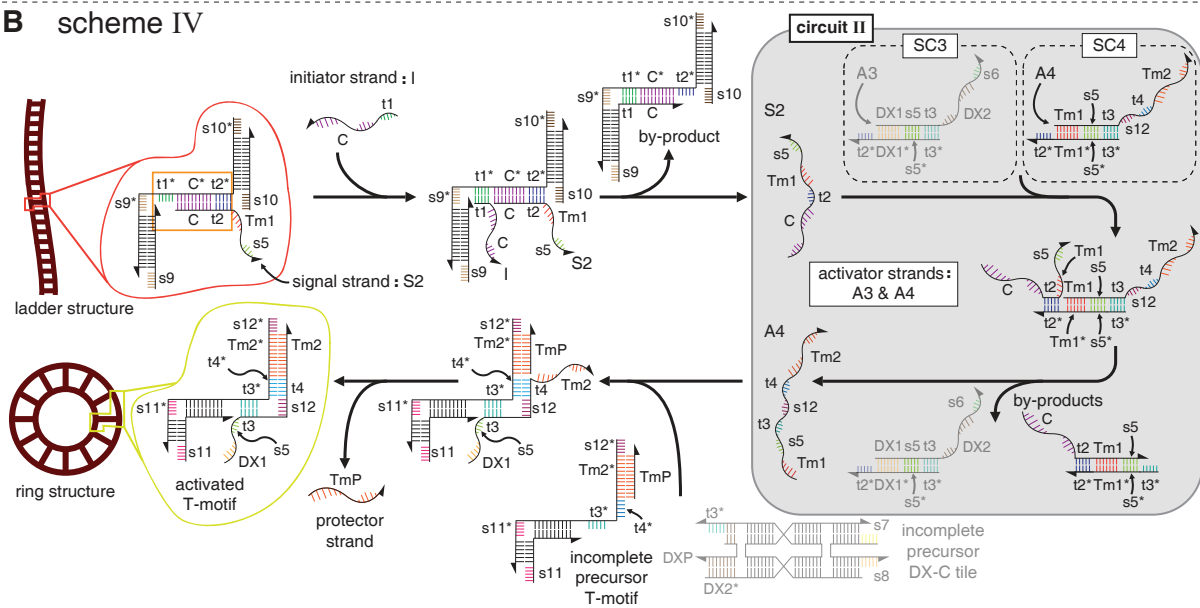


Figure 3: Schematics of schemes III and IV. **a** Details of scheme III. The initial T-motifs making up the initial ladder structure have an exposed $t1^*$ toehold domain (boxed in orange). The reaction cascade starts when the initiator strand I ($t1$ -C) is inserted into the system and its $t1$ domain hybridizes with the $t1^*$ toehold domain of the initial T-motif, which facilitates branch migration of the C domain to displace the signal strand S2 (C- $t2$ -Tm1- $s5$). This signal strand activates circuit I which includes two subcircuits, SC1 and SC2, who share a common toehold $t2^*$ but are otherwise sequentially orthogonal. The signal strand can bind to the toehold of either SC1 or SC2 but branch migration only occurs for SC2, since it is the only one with a common DX1 branch migration domain. The signal strand then activates SC2 which produces the activator strand A2 (Tm1- $s5$ - $t3$ -DX2- $s6$) through strand displacement. After binding at the $t3^*$ toehold domain, this A2 activator strand provides the missing $s5$ and $s6$ sticky-ends. The $s6$ sticky-end is provided by displacing the DXP protector strand. This activates the DX-C tile and allows for sticky-end bindings with DX-D tiles to produce DX-II lattices. **b** Details of scheme IV. The reaction cascade up to the production of the signal strand S2 is the same as scheme III. Activation of SC4 produces a displaced activator strand A4 (Tm1- $s5$ - $t3$ - $s12$ - $t4$ -Tm2) which binds to an incomplete precursor T-motif at the $t3^*$ and $t4^*$ toehold domains. Without the A4 activator strands, these precursor T-motifs cannot self-assemble into higher-order structures due to the missing $s12$ sticky-end. The domain between the $t3$ and $t4$ domains of the invading A4 activator strand provides this missing $s12$ sticky-end. Once bound at these toehold domains, the A4 strand displaces the TmP protector strand to complete the formation of a new T-motif which self-assembles into a ring structure. All functional domains are colour-coded and labeled; their complementary counterparts are starred (e.g. Tm1 and Tm1*). Half-arrowheads on the strands indicate the 3' direction. Components shown at half opacity stay non-reactive for that particular scheme.

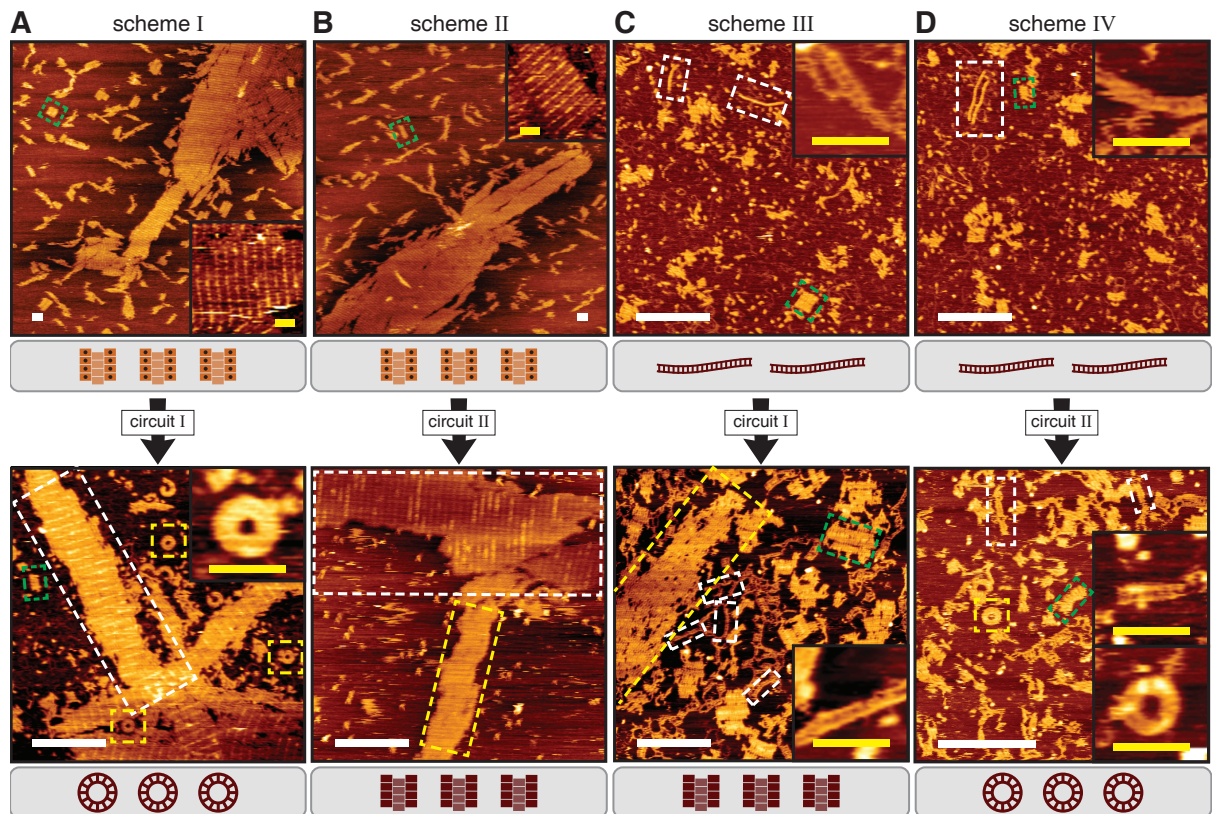


Figure 4: AFM data of the (top row) initial and (bottom row) final output structures. **a** Scheme I. (Top row) The initial DX-I lattices where the bright stripes are the columns of hairpins. (Bottom row) The self-assembled output ring structures (dashed yellow box) as well as the remaining initial DX-I lattices (dashed white box). **b** Scheme II. (Top row) The same initial DX-I lattices. (Bottom row) The output DX-II lattices (dashed yellow box) and remaining DX-I lattices (dashed white box). The two types of lattices can be distinguished by the presence (DX-I) or absence (DX-II) of hairpin stripes. **c** Scheme III. (Top row) The initial ladder structures (dashed white boxes) and (bottom row) their output DX-II structures (dashed yellow box). **d** Scheme IV. (Top row) The same initial ladder structure (dashed white box) and (bottom row) their output ring structures (dashed yellow box). Some of the images show dashed green boxes which enclose small fragment DX structures formed from bindings between incomplete precursor DX-C tiles and DX-D tiles existing in the system (see Fig. 5 d and Supplementary Fig. 8). Insets show magnified views of some of the structures. (White scale bars : 200 nm; inset yellow scale bars : 50 nm)

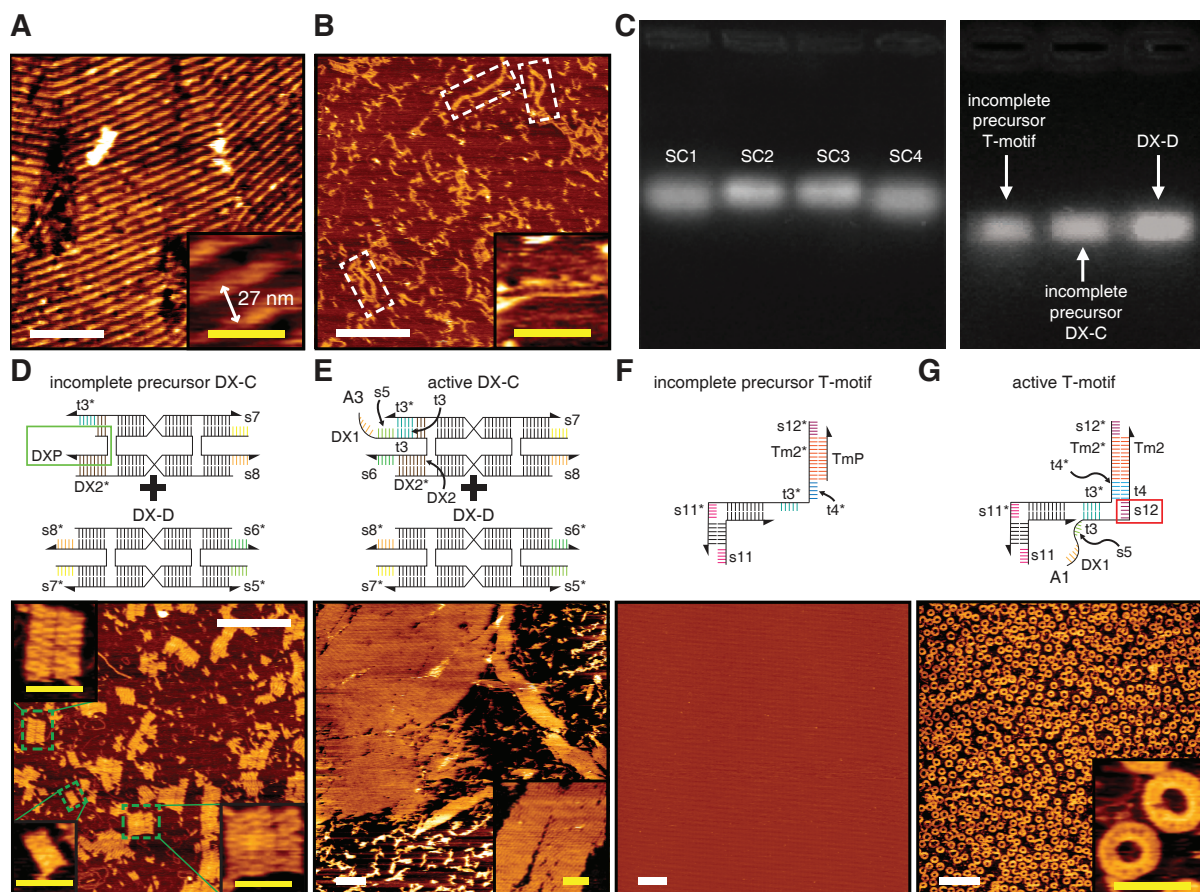


Figure 5: Control and purification data. AFM data of the initial structures after spin filtration, **a** DX-I lattices used in schemes I and II and **b** ladder structures used in schemes III and IV. These two images were obtained prior to adding the other components to the system (*e.g.* DNA circuit components and precursors). The dashed white boxes in **b** show typical ladder structures. **c** Agarose gel electrophoresis data of (left) the DNA subcircuits and (right) other motifs used in the experiments. These bands were excised and their products purified and used in schemes I-IV (see Methods). **d** Unwanted bindings between incomplete precursor DX-C and DX-D tiles forming small fragment DX lattices. Although precursor DX-C tiles lack s5 and s6 sticky-ends (green box), some bindings between s7, s8, and their complementary sticky-ends occur to form small fragments having widths of (insets) 2-, 4-, and 6-tiles wide (Supplementary Fig. 8). Although it is not too common to find these types of unwanted fragments in schemes I-IV, this image was taken with a sample made from over ~ 13 times the molar concentration of those used in our schemes (400 nM here as opposed to 30 nM samples used in schemes I-IV) to emphasize this phenomenon. The fragments found in our experiments do not seem to interfere with the intended reaction pathway. **e** DX-II lattices self-assembled from active DX-C tiles, where the protector DXP strand, green box in **d**, has been replaced with the A3 activator strand. AFM images of **f** incomplete precursor T-motifs, which cannot form rings due to missing s12 sticky-ends, and **g** well-formed ring structures where the A1 activator strand has been added to activate the T-motif by providing the missing s12 sticky-end (red box). Due to the kink in the spoke of the T-motif, the number of motifs that make up each ring structure (~ 20) is a bit higher than conventional T-motif rings ($\sim 12-16$).¹⁴ The samples used in **d** - **g** were separately prepared in a one-pot annealing procedure with their respective components at a molar concentration of 400 nM and did not undergo the strand displacement reactions. (White scale bars : 200 nm; inset yellow scale bars : 50 nm)